Temporal-spatial variation of wave energy and nearshore hotspots in the Gulf of Oman based on locally generated wind waves

Bahareh Kamranzad[a*], Vahid Chegini[a] and Amir Etemad-Shahidi[b]

[a] Ocean Engineering and Technology Research Center, Iranian National Institute for Oceanography and Atmospheric Science, Tehran, Iran, Tel: +98-21-66944873, Fax: +98-21-66944869

*Corresponding author e-mail: kamranzad@inio.ac.ir,

v_chegini@inio.ac.ir

[b] Griffith School of Engineering, Gold Coast campus, Griffith University QLD 4222, Australia, Tel: +61-07-5552 9267, Fax: +61-07-5552-8065

E-mail: a.etemadshahidi@griffith.edu.au

Abstract

This study aims to assess the wave energy at five coastal stations in the Gulf of Oman using the time series of locally generated wind waves obtained by numerical modeling for 11 years. For this purpose, the spatial, seasonal, monthly, directional, inter-annual of wave energy and power were investigated. The spatial distribution shows that the wave power increases towards the Indian Ocean and the highest mean wave power is located at the eastern station in all seasons. In addition, monthly mean wave power is highest during July and August while the monthly maximum wave power is highest during February at all stations. The ratio of monthly maximum to mean wave power is also the lowest during May to August. Moreover, Monthly Variability Index is the

highest in west of the domain where there is no significant wave power potential. In addition, annual wave power as well as total and exploitable wave energies increases from west to east, where the dominant waves propagate from the south, and the exploitable wave energy is approximately 20 times greater than of the central stations.

Keywords: wave power; exploitable wave energy; seasonal and monthly distributions, monthly variability index

1. Introduction

In recent decades, fossil fuels have caused the increasing in emission of greenhouse gases which have resulted in increasing the earth's temperature, and consequently, the climate change impacts. Fossil fuels are non-renewable and will be finished in near future. Therefore, renewable energy resources are alternatives for reducing the greenhouse gases' emission and confronting the impacts of using fossil sources. Marine energies are vast and largely untapped resources of renewable energies in countries surrounding the seas and oceans. As well as the fact that the wave energy contains the highest energy density among the other marine renewable energy resources [1], predictability and low visual and environmental impacts make the wave energy a valuable renewable energy resource [2]. Many studies have focused on the study of wave energy potential in various locations all around the world, e.g. Atlantic coast of Europe [2-8], Mediterranean Sea [9,10], China Sea [11,12], Bohai and Yellow Sea [13], Indian shelf seas [14], around Hawaii [15,16], U.S. Pacific northwest [17,18], Baltic Sea [19], Caspian Sea [20-23] and Persian Gulf [24,25] and many other locations.

In this study, wave energy is assessed in coastal areas of the northern Gulf of Oman.

The Gulf of Oman, as an extension of Indian Ocean, connects the Persian Gulf to the Arabian Sea and Indian Ocean. In addition, because of its natural geographic location, northern coasts of Gulf of Oman are potential hubs for marine transport. For example, Chabahar port, located in the northern part of Gulf of Oman, is a free trade-industrial zone and any development of industries increases the energy demand there. This energy demand can be supplied by available wave energy as a clean and green renewable energy resource. Since the Gulf of Oman is located in north of the Arabia Sea and Indian Ocean, a considerable energy from the waves enters the domain, mainly due to the monsoon events taking place.

Therefore, in this study wave energy potential is assessed along some coastal stations located in the northern Gulf of Oman based on the wave characteristics obtained from the wave modeling. The aim of this study is to locate the most appropriate locations for wave energy extraction between selected coastal stations with high density population along the northern coasts of the Gulf of Oman. A prior study has been carried out by Saket and Etemad-Shahidi [26] in the north-eastern parts of the Gulf of Oman in which the computational area covered only bay of Chabahar (Fig. 1) as a part of Gulf of Oman. Our study aims to estimate and assess the wave energy potential not only around Chabahar area, but also in the Gulf of Oman and some other coastal areas from a different viewpoint, i.e.; temporal-spatial distributions and the available and exploitable wave energy. The paper is arranged as follows: Section 2 introduces the material and methods, including the study area and data resources; Section 3 consists of results and discussion on wave power distribution in the domain and coastal areas, temporal and directional distributions of the wave power with inter-annual variations of the wave energy; Section 4 includes the summary and conclusions.

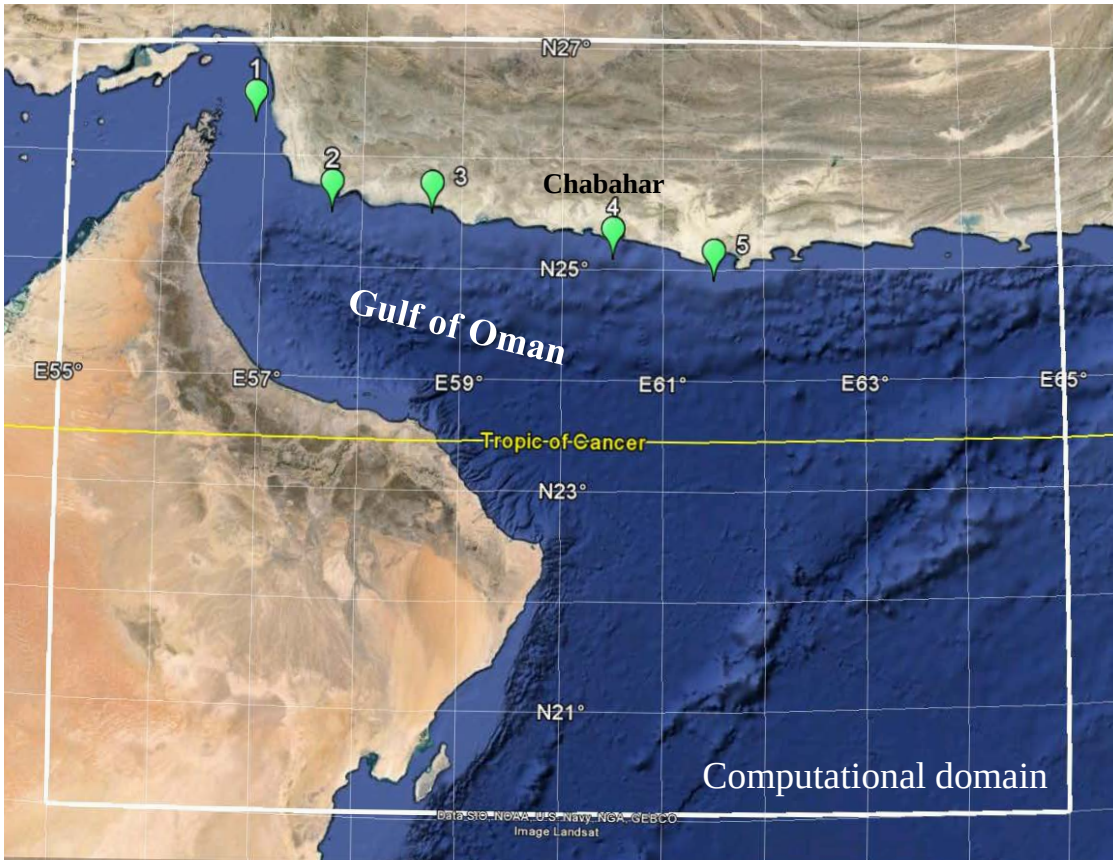

Fig. 1. Location of Gulf of Oman, computational grid and selected stations

2. Materials and methods

Wave modeling was carried out using SWAN (Simulating WAves Nearshore) numerical model [27]. This model has been used extensively for modeling of wave climate in semi enclosed areas [e.g. 25,28,29]. SWAN is a spectral model developed for estimation of the wave characteristics, especially in nearshore areas. This model considers the governing processes for small scale, high resolution applications such as generation, dissipation and nonlinear wave-wave interactions [30].

The basic equation used in the SWAN is the action balance equation which for the Cartesian coordinates is as follows [30]:

$$\frac{\partial}{\partial t}N+\frac{\partial}{\partial x}c_x N+\frac{\partial}{\partial y}c_y N+\frac{\partial}{\partial \sigma}c_\sigma N+\frac{\partial}{\partial \theta}c_\theta N=\frac{S}{\sigma} \quad (1)$$

in which, N shows the action density and is a function of intrinsic frequency (σ), wave direction (θ), horizontal coordinates (x and y) and the time (t). The first term on the left-hand side represents the temporal change of N. The next two terms show the propagation of N in geographical x and y space, respectively (in which, c_x and c_y are the propagation velocities in x and y directions, respectively) while the fourth term depicts the shifting effect of the relative frequency due to variations in depth and currents (in which, c_σ shows the propagation velocity in σ space). The last term on the left-hand side shows the depth and current-induced refraction (in which, c_θ shows the propagation velocity in θ space). The term S on the right-hand side of the equation is a function of σ, θ, x, y and t and consists of effects of the generation by wind, dissipation (by white-capping, depth induced wave breaking and bottom friction) and nonlinear wave-wave interactions [30].

In this study, SWAN was executed in the third generation and two dimensional nonstationary mode and the theory of Komen et al. [31] wind input parameterization was used. In addition, whitecapping, nonlinear wave interactions, breaking and friction were also activated to be considered in case they are applicable. The computational time step was selected as 10 minutes and the model outputs were also produced in a 0.2 degree (about 20 km) resolution in the computational domain (Fig. 1) with a time step of 3 hrs.

The wind field utilized for wave modeling was ECMWF (European Centre for Medium-Range Weather Forecasts) with 0.5º spatial and 6 hr temporal resolutions available from 1992 to 2003, containing both reanalysis (1992 to 2002) and operational (2002 to 2003) products. This dataset has been modified and localized in the domain in the previous studies [e.g .32] and has been successfully used for

prediction of wave height and extreme value analysis in this area [33,34]. Hence, it was used in this study in order to model the wave characteristics, as well. Although the extreme values of the wave characteristics may be underestimated due to the underestimation of ECMWF strong winds [35-37], their contribution to mean wave energy due to their low frequency of occurrence can be neglected. Bathymetry data were also obtained from NOAA's National Geophysical Data Center (NGDC) website, with a spatial resolution of 1 min (about 1.67 km in the study area). Wave data recorded by a buoy located in Chabahar, north of Gulf of Oman, at 60.65º E and 25.267º N (near the Chabahar port), in a depth of about 17 m, were used for the calibration and verification of the numerical model.

Model calibration and verification were carried out based on the minimizing the errors for wave power parameter, rather than significant wave height and wave period. Long term wave energy estimation was carried out using significant wave height and period [32,38]. The wave energy density is calculated from Eq. (2) [39].

$$E = \frac{1}{16}\rho g {H_s}^2 \tag{2}$$

in which ρ, g and H_s illustrate the water density, gravitational acceleration and significant wave height (in meter), respectively. Therefore, the wave power is defined as:

$$P = EC_g = ECn \tag{3}$$

In which C represents the wave speed and n is the ratio of wave group speed to the wave speed (it is approximately equal to 0.5 in deep water). C is equal to wave length divided by the wave period (T) and the wave length is equal to $gT^2/2\pi$ in deep water. Therefore, the wave power is calculated as follows.

$$P = \frac{1}{16}\rho g H_s^2 \times \frac{gT}{2\pi} \times 0.5 \approx 0.49 H_s^2 T \tag{4}$$

The real sea states include a large number of regular waves. Therefore, a mixture of different amplitudes, frequencies and directions is described using a variance spectral density function. The wave power per unit width of the irregular waves in deep water is obtained by [32]:

$$P = \approx 0.49 H_s^2 T_e \tag{5}$$

in which T_e is the energy period and is equal to T_p multiplied by a factor. For a standard JONSWAP spectrum with a peak enhancement factor of γ=0.33, the factor will be equal to 0.9 [32]. Since the peak period was reported, it was also obtained from the numerical model in order to calibrate and verify the results.

As mentioned before, calibration of SWAN model was carried out based on minimizing the errors for the modeled wave power. Following Saket and Etemad-Shahidi [26], three weeks were considered for the calibration period (from Feb., 16, 2000 to Mar., 7, 2000) and two weeks were considered for the verification period (Jan., 20, 1999 to Feb., 3, 1999) (see also [22,25]). The selection of these periods was based on the data availability. For quantitative assessment of the calibration results, error indices, i.e. *Bias*, correlation coefficient (*CC*) and root mean square error (*RMSE*) were calculated as follows:

$$Bias = \bar{y} - \bar{x} \tag{6}$$

$$CC = \frac{\sum_i ((x_i - \bar{x}) \times (y_i - \bar{y}))}{\sqrt{\sum_i (x_i - \bar{x})^2 \sum_i (y_i - \bar{y})^2}} \tag{7}$$

$$RMSE = \sqrt{\frac{\sum_i (x_i - y_i)^2}{n}} \tag{8}$$

in which, x_i and y_i denotes the measured and modeled values, respectively. $\bar{x}$ and $\bar{y}$ are their average values, respectively.

To confirm the reliability of the model, it was validated in the verification period without changing the coefficients that were optimized in calibration period using error minimization. Statistical parameters of significant wave height and wave period in the calibration and verification periods are shown in Table 1. According to this table, the wave statistics are nearly similar in the calibration and verification periods, and the longest wave period in the considered five weeks is about 8 s, which implies the prevalence of seas. Therefore, the swells were not considered in wave power estimations due to their low occurrence frequency in this region (see also Saket and Etemad-Shahidi [26]) and only locally generated wind waves (seas) were considered for wave energy estimations.

Table 1. Statistical wave parameters for calibration and verification

Parameter	Period	Minimum	Average	Maximum	Standard deviation
Significant wave height (m)	Calibration	0.25	0.57	1.62	0.25
	Verification	0.18	0.47	1.59	0.24
Wave period (s)	Calibration	3.60	5.02	8.00	0.91
	Verification	2.65	3.60	4.72	0.45

Fig. 2 and Table 2 show the results of model verification. According to Table 2, there is an acceptable agreement between the modeled and measured values of the wave power. Since the ECMWF wind field underestimates strong winds, some peaks are underestimated in time series of the modeled wave power shown in Fig. 2. However, Model calibration and verification were carried out based on the minimizing the error measures for the total period and not only the peak values. Therefore, this model was utilized to produce the wave power time series in the Gulf of Oman.

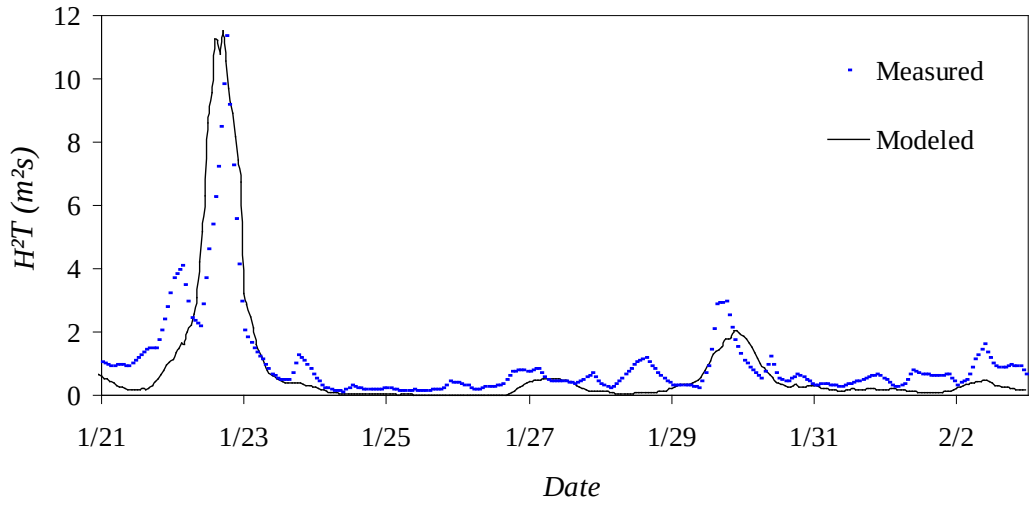

Fig. 2. Time series of modeled and measured H_s^2T, verification period

Table 2. Error indices for H_s^2T for calibration and verification

Error Index	Calibration	Verification
Bias (kW/m)	-0.007	-0.236
CC	0.884	0.896
RMSE (kW/m)	2.274	0.908

3. Results and Discussion

3.1. Wave power distribution in the domain

Wave power was calculated from the time series of wave characteristics generated by numerical modeling for 11 years for all output grid points. Fig. 3 shows the seasonal distribution of the wave power in the Gulf of Oman. According to this figure, the wave power increases moving from the north western areas (Strait of Hormuz) towards the south eastern areas (Indian Ocean). Furthermore, the highest mean wave powers are approximately 1.3, 2.3, 5.3 and 0.8 kW/m for winter, spring, summer and autumn, respectively that imply the highest and lowest wave power values exist in

summer (concurrent with the monsoon period) and autumn, respectively. This is in line with the previous findings of Saket and Etemad-Shahidi [26], focusing on Chabahar region. In the eastern parts of the domain, the spring mean wave power is higher than that of winter; while in the western areas, the winter wave power is higher than that of spring.

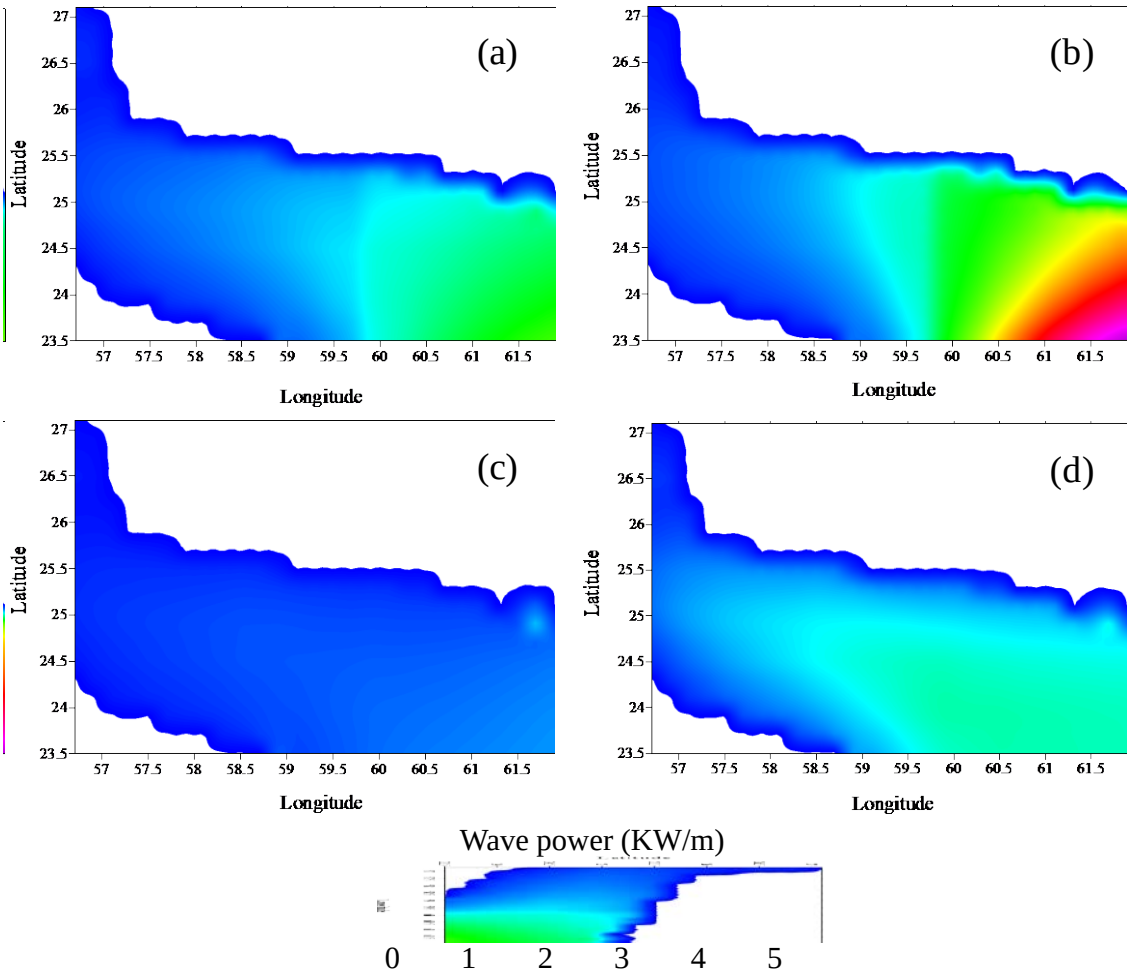

Fig. 3. Wave power (kW/m) distribution in Gulf of Oman in (a) Spring, (b) Summer, (c) Autumn and (d) Winter

3.2. Wave power distribution in coastal areas

Evaluation of wave power potential in coastal areas helps the planning for extracting the energy from the waves. For this purpose, five coastal stations were selected in

northern areas of Gulf of Oman, and their wave power data were obtained based on the results of wave modeling. These stations named Sirik, Jask, Googsar, Chabahar and Govatr (stations 1 to 5 located from west to east, respectively) are shown in Fig. 1 and Table 3. In the next sections, their seasonal, monthly, directional, inter-annual and storage of wave energy will be discussed in detail.

Table 3. Selected stations and wave power characteristics

Station ID	Station no.	Long. (deg)	Lat. (deg)
Sirik	1	56.9	26.3
Jask	2	57.7	25.5
Googsar	3	58.7	25.5
Chabahar	4	60.5	25.1
Govatr	5	61.5	24.9

3.2.1. Seasonal distribution of wave power

Seasonal variations of mean and maximum wave power in five stations are shown in Fig. 4. According to this figure, the highest mean wave power exists at station 5 in all seasons. In addition, during autumn, winter and spring, the mean wave power increases gradually from west (station 1) to east (station 5) of the domain. However, during summer, the increase of mean wave power at stations 4 and 5 is considerable. This may be due to the summer monsoon affecting the east parts of the Gulf of Oman adjacent to the Arabian Sea and Indian Ocean. The lowest mean wave power in all stations occurs during autumn. In addition, in stations 1 to 3, the winter wave power is higher than the spring wave power which is similar to the results obtained in section 3.1. The annual mean wave power value is similar to the wave power during spring. It

is obvious that the annual wave power varies according to the wave power increasing from west to east, in all seasons.

The seasonal distributions of wave power show a significant seasonal variation at stations 4 and 5. For example, it ranges from approximately 0.3 and 0.8 kW/m in autumn and winter, respectively to approximately 1.3 and 2.6 kW/m in spring and summer, respectively. This means that more than 8 times increase in wave power in summer compared to that of autumn.

The maximum wave power, which is due to the occurrence of storm events, is highest in winter at all stations and ranges from approximately 34 kW/m at station 3 to approximately 51 kW/m at station 1. After the maximum winter wave power, the highest maximum seasonal wave powers exist in spring at stations 1 to 3 (with values of approximately 15, 19 and 14 kW/m, respectively) and in summer at stations 4 and 5 (with values of approximately 20 and 30 kW/m, respectively).

The maximum wave power is also higher at station 5 in all seasons except for winter when the maximum wave power is highest at station 1. Moreover, the maximum wave power is the lowest during summer at stations 1 to 3 and during autumn in stations 4 and 5.

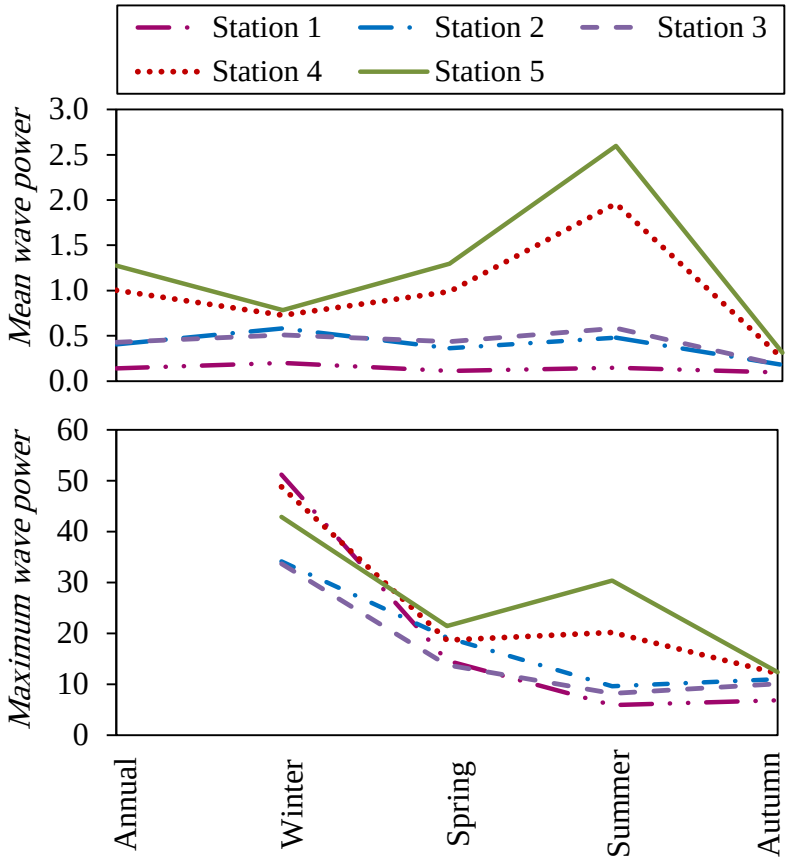

Fig. 4. Seasonal and annual distributions for (a) mean and (b) maximum wave power (kW/m)

3.2.2. Monthly distribution of wave power

Fig. 5 shows the monthly distribution of mean, maximum and the ratio of maximum to mean wave power. This figure represents that the monthly mean wave power is highest during Jan to March at stations 1 to 3 and during June to August at station 4 and 5 while the monthly maximum wave power is highest during February at all stations. There is an increase of maximum wave power in June at station 1 which is located in the western part of domain in the vicinity of the Persian Gulf where it is affected by the prevailing winds during this period called Shamal winds [40]. Comparison of monthly wave power in different stations indicates that the highest and lowest values occur mostly at stations 5 (approximately 3.2 kW/m in July) and 1

(approximately 0.12 kW/m in October), respectively. This figure also illustrates significant monthly variations at stations 4 and 5. For example, the wave power varies between 0.28 and 3.2 kW/m at station 5 which implies that the mean wave power is approximately 11.5 times greater in July than October.

Fig. 5-c represents the ratio of monthly maximum to mean wave power. The lowest ratio implies the lowest variability of the wave power in a month. Regarding Figs. 5-a and 5-b, the difference between maximum and mean wave power is very large at station 1. For example, it is approximately 228 in June where the mean and maximum wave powers are about 0.2 and 45.7 kW/m, respectively. Since this is very different from the ratio at other stations and considering the low amount of wave power in this station, it was excluded from Fig. 5-c. Fig. 5-c also shows the lowest ratios exist during May to August and the wave power ratio varies slightly during these months. This ratio increases during November and February in all stations and also during April in stations 2 and 3 , implying a high variation of wave power range.

To determine the monthly variability of wave power and to evaluate the stability of the calculated monthly wave power, Monthly Variability Index (MVI) is used [41,42]. The MVI is the ratio of the difference between the maximum and minimum monthly mean wave power and the annual mean wave power [14]. Table 4 shows the mean monthly, annual and MVI values for all stations during 11 years. According to this table, the MVI values range between 1.26 at station 3 to 2.41 at station 1.Sanil Kumar and Anoop [14] also assessed the wave energy resources in the Indian shelf seas and estimated the MVI varies from 1.5 to 3. Zhou et al. [12] also represented the temporal (annual, seasonal and monthly)-spatial distribution of wave energy in Beibu Gulf, China and indicated that the maximum MVI is about 1.1 that implies a stable monthly wave condition. Therefore, based on mean annual wave power and MVI values (Table

4), the most inappropriate place for wave energy extraction is station 1 in which the lowest wave energy and highest MVI can be seen.

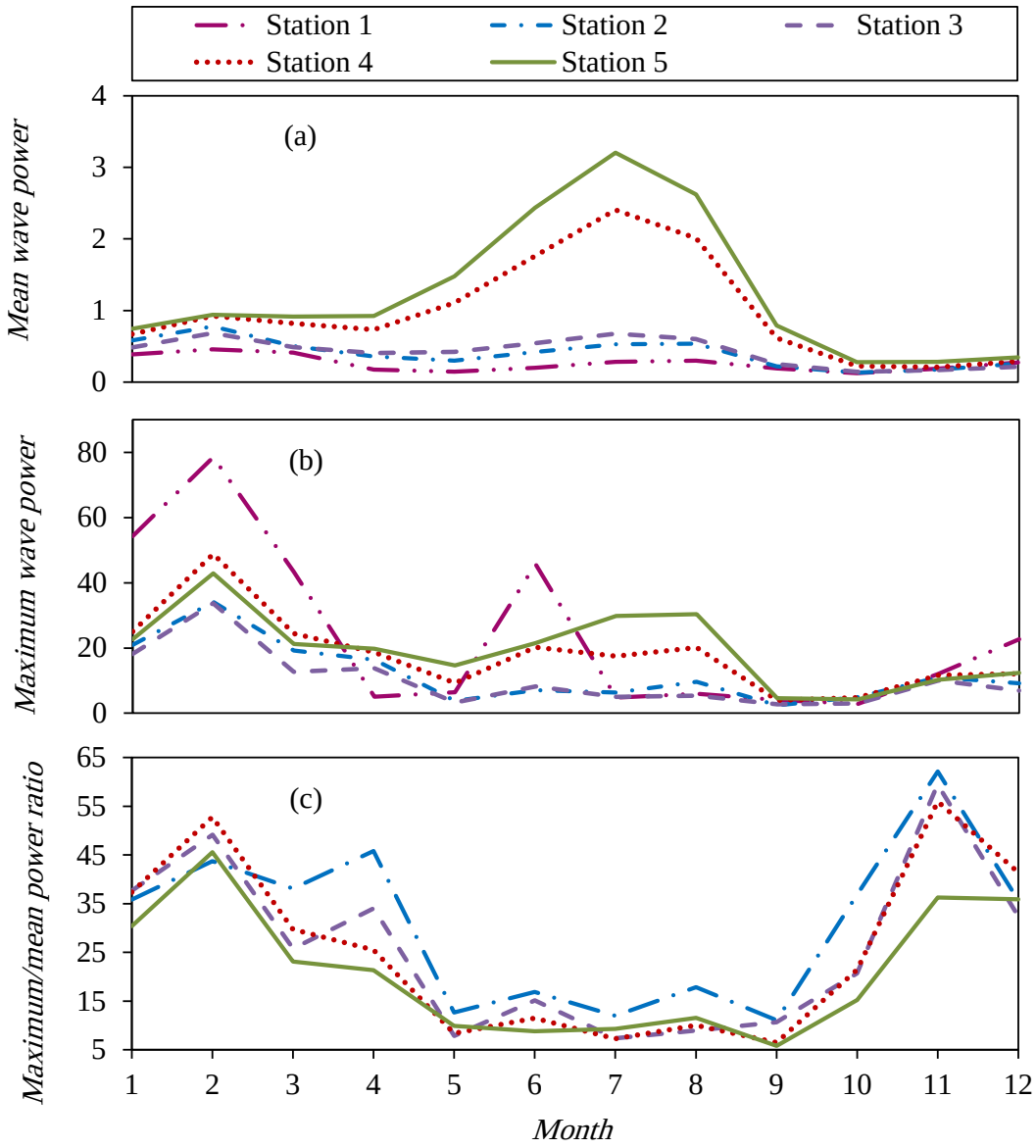

Fig. 5. Monthly distributions for (a) mean, (b) maximum and (c) ratio of Maximum/mean wave power (kW/m)

Table 4. Monthly and annual mean wave power and Monthly variability index

Station no.	Mean wave power (*kW/m*)													Monthly variability index
	Jan	Feb	Mar	Apr	May	Jun	Jul	Aug	Sep	Oct	Nov	Dec	Mean annual	
1	0.39	0.46	0.41	0.17	0.15	0.20	0.29	0.30	0.19	0.12	0.19	0.27	0.14	2.41
2	0.59	0.78	0.50	0.36	0.30	0.42	0.53	0.54	0.22	0.13	0.18	0.26	0.40	1.60
3	0.48	0.69	0.49	0.40	0.42	0.54	0.68	0.60	0.25	0.15	0.17	0.21	0.43	1.26
4	0.67	0.92	0.82	0.73	1.11	1.76	2.41	2.01	0.62	0.22	0.21	0.29	1.00	2.19
5	0.75	0.94	0.92	0.93	1.48	2.44	3.21	2.62	0.79	0.28	0.28	0.34	1.28	2.30

3.2.3. Directional distribution of wave power

Directional distribution of the wave propagation for different intervals of wave power values are shown in Figs. 6-10 using wave power roses of five stations. According to these figures, the dominant annual wave direction is W-SW at station 1, SE at station 2, W at station 3 and S at stations 4 and 5. The dominant wave direction in most of the stations is S or SE in summer due o the waves coming from the Indian Ocean, and it changes during the other seasons. In addition, the dominant wave direction varies from W-SW, W-NW and W at western stations to S and S-SW at eastern stations in spring. In summer, the dominant wave direction in western stations rotates to SE (except for station 1) and the south waves are dominant at the eastern stations.

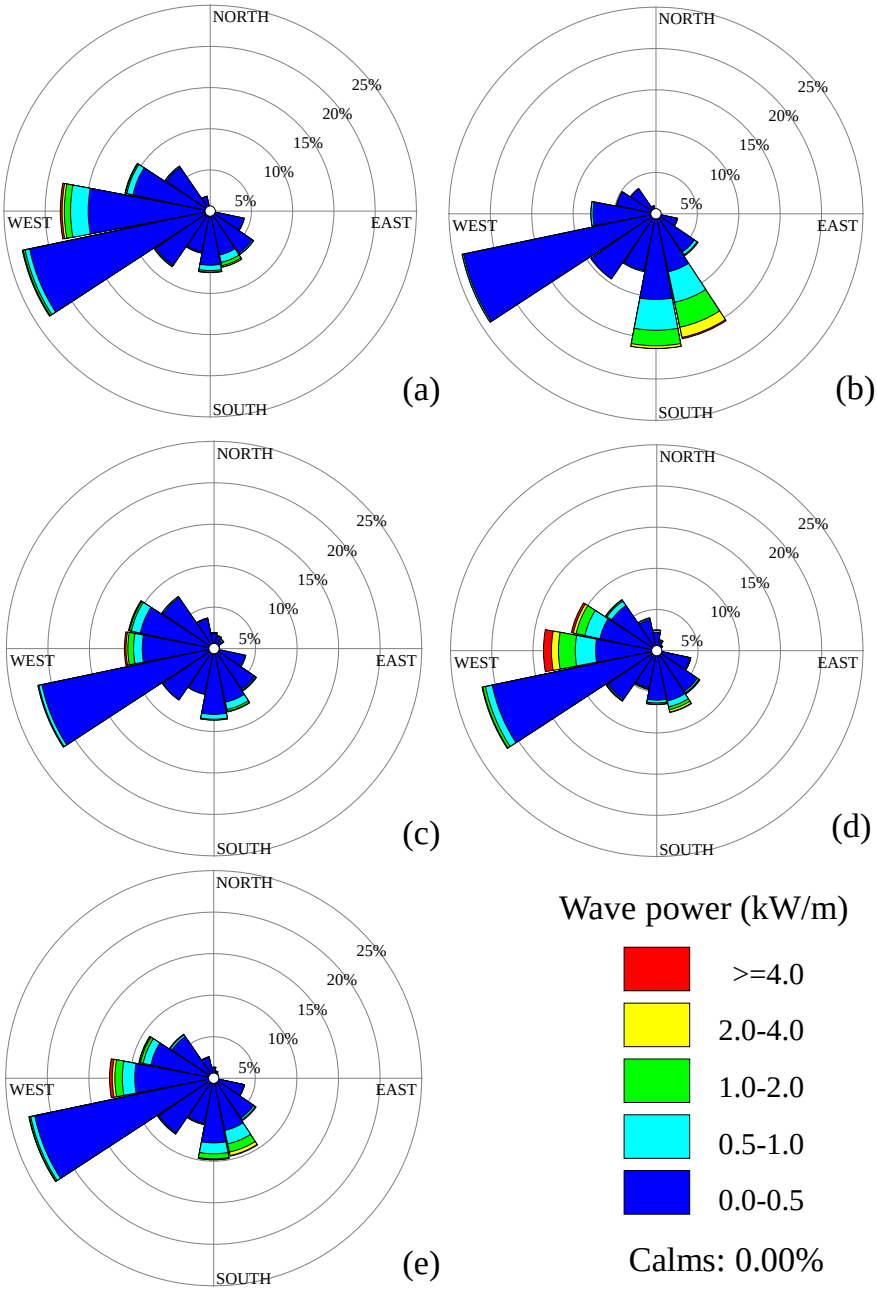

Fig. 6. Wave power roses, (a) spring, (b) summer, (c) autumn, (d) winter and (e) annual, in station 1

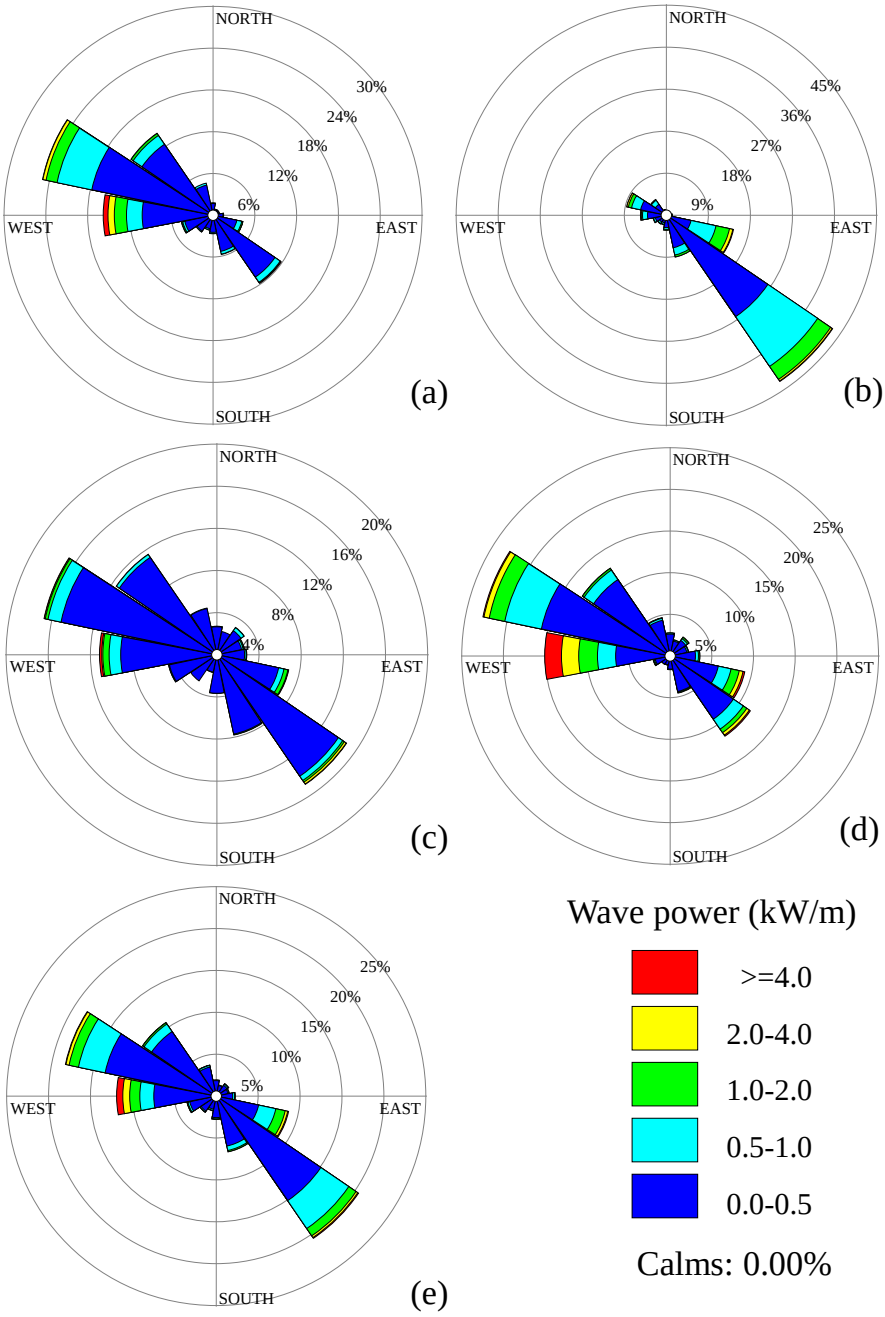

Fig. 7. Wave power roses, (a) spring, (b) summer, (c) autumn, (d) winter and (e) annual, in station 2

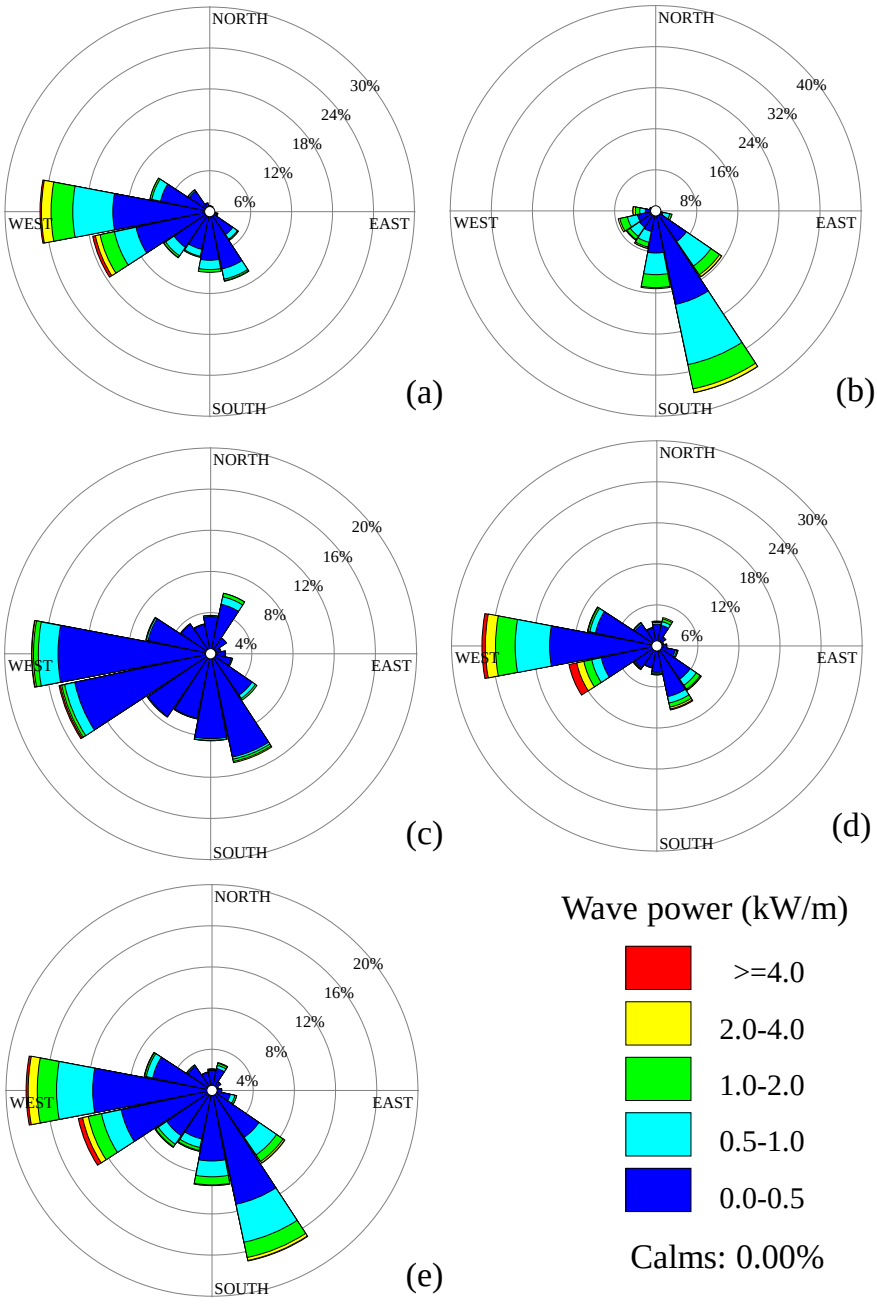

Fig. 8. Wave power roses, (a) spring, (b) summer, (c) autumn, (d) winter and (e) annual, in station 3

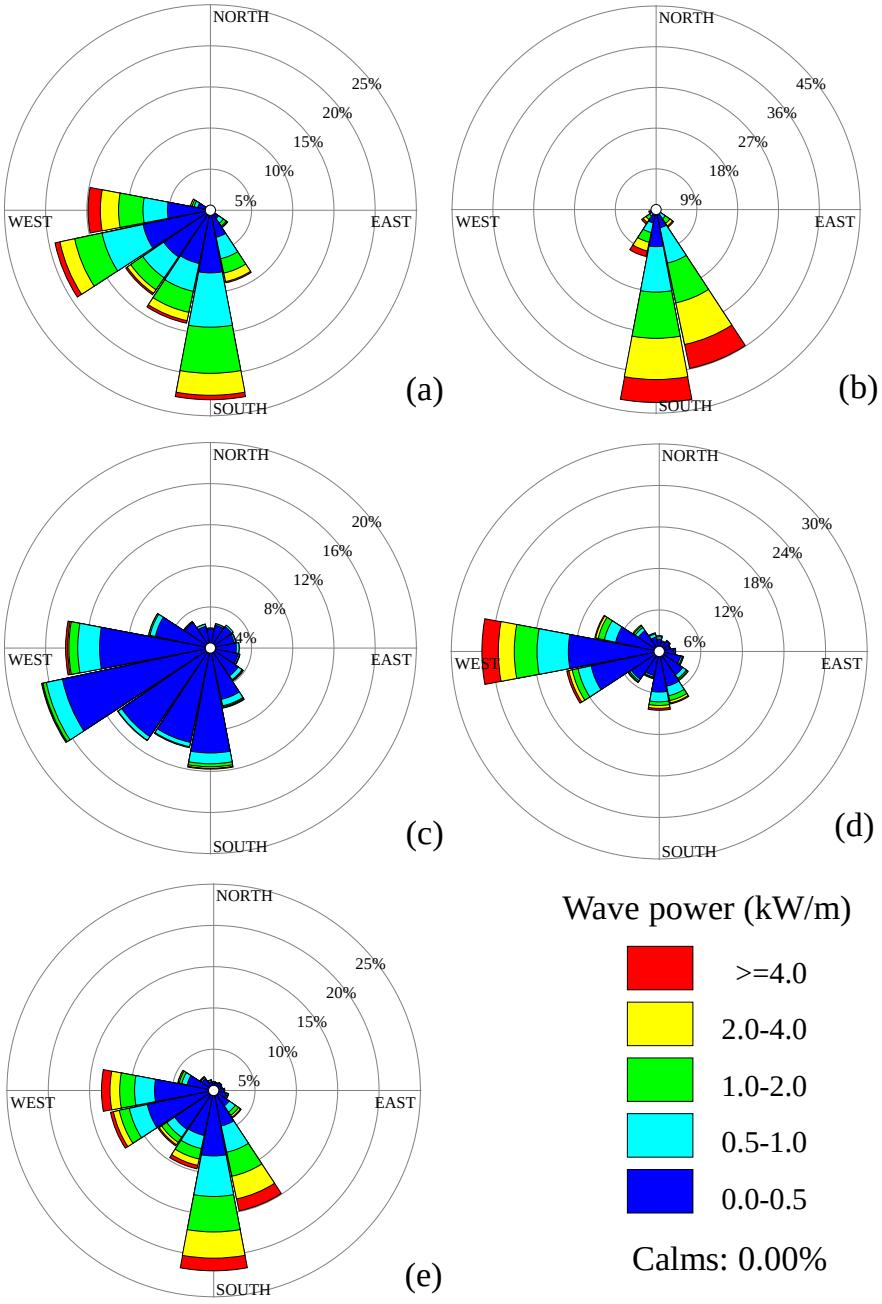

Fig. 9. Wave power roses, (a) spring, (b) summer, (c) autumn, (d) winter and (e) annual, in station 4

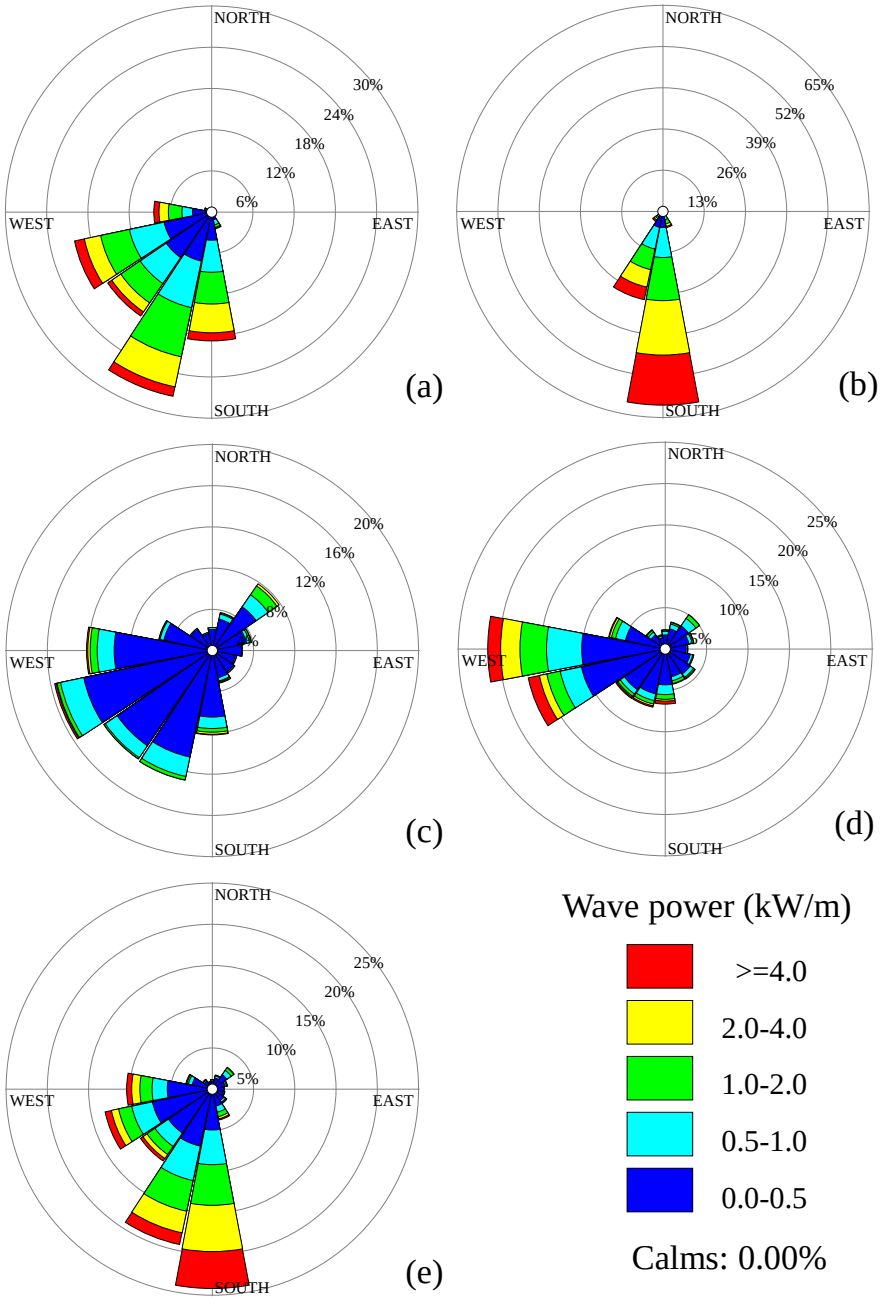

Fig. 10. Wave power roses, (a) spring, (b) summer, (c) autumn, (d) winter and (e) annual, in station 5

3.2.4. Inter-annual variations in wave power

Assessment of inter-annual variation of the wave power is required to ensure the stable wave energy, and it has been carried out in many studies (e.g. [14,25,43]). Therefore, in order to analyze the long term variation of wave power, inter-annual

variation of the mean wave power was also investigated. Fig. 11 shows the inter-annual trend of mean annual and seasonal wave power during 1992 to 2002. This figure illustrates a slight increase and then a slight decrease of mean annual wave power during 1992 to 1996 and 1997 to 2001 at stations 2 to 5.

The annual variation of mean wave power is nearly similar to those of the spring, summer and autumn trends for these stations while the winter trend is different. Comparison between inter-annual variations of wave power in all stations indicates that the highest annual wave power always occurs at station 5 in all years except for winter 1992 when the wave power was higher at station 2; while generally, the lowest wave power has occurred in station 1 during this period. In addition, the mean annual and seasonal wave power values are nearly similar in stations 2 and 3 during 1992 to 2002. In addition, the highest variations of the annual wave power occur at stations 4 and 5 and seasonal comparison also shows the highest variations during winter.

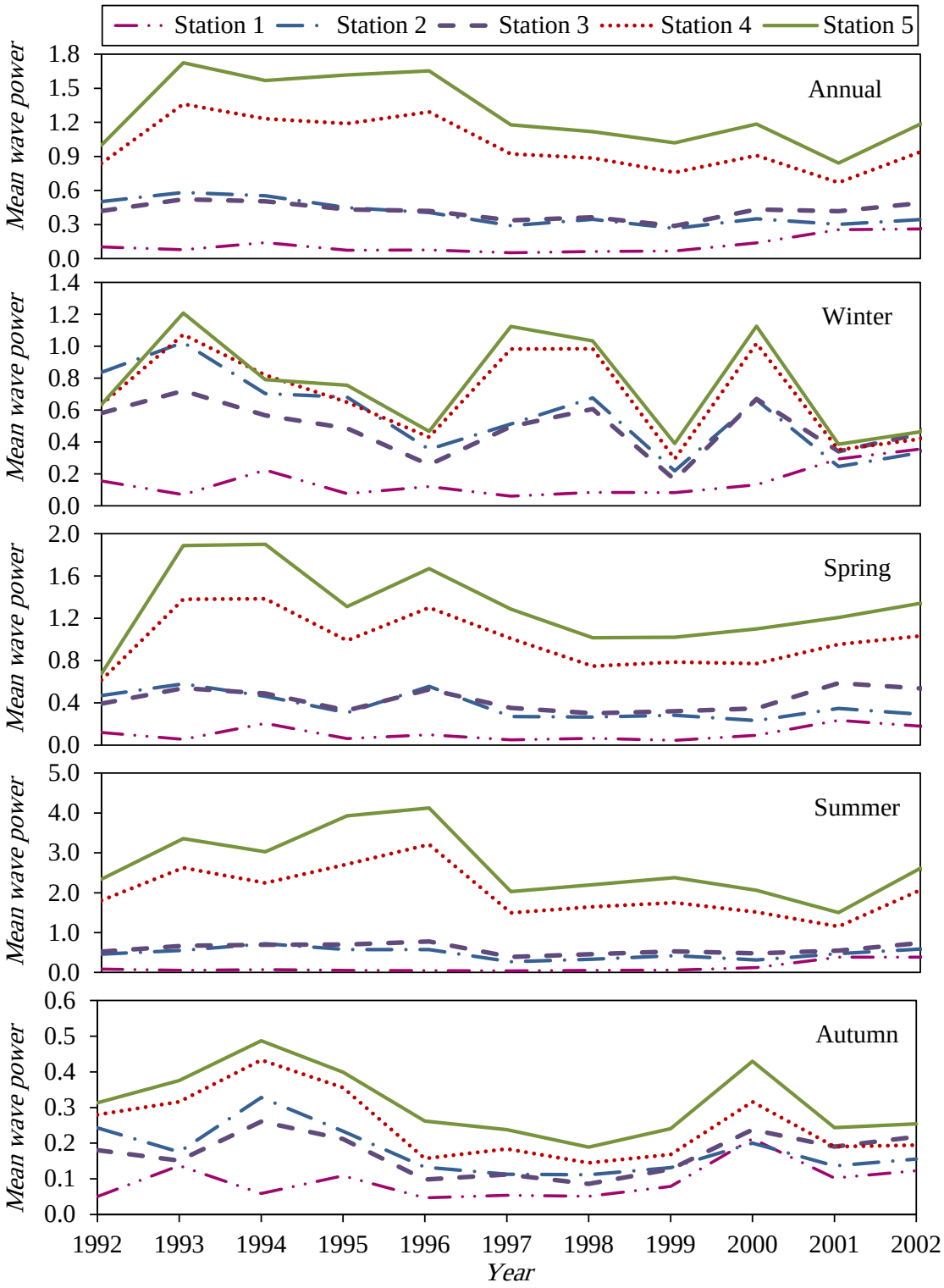

Fig. 11. Inter-annual distributions of seasonal mean wave power (kW/m)

3.2.5. Wave energy potential

Two indices are generally used for evaluation the potential value of wave energy converter deployment consisting of the total and exploitable storage of wave energy, according to equations 8 and 9.

$$E_t = P_{mean} \times t \quad (8)$$

$$E_e = P_{mean} \times t_e \quad (9)$$

In which E_t and E_e represent the total and exploitable storage per unit area, respectively while t shows the total hours all year round (=8760 hr), t_e shows the exploitable time per unit area in theory, which means the corresponding hours to wave power value greater than 2 kW/m. This threshold was used to estimate t_e because the wave energy worth exploitation when it is greater than 2 kW/m [42,44].

Table 5 shows the total and exploitable wave energy values at different stations. According to this table, the total and exploitable wave energies increase from west to east and the richest wave energy is located at station 5 at the east of the domain where the total and exploitable storages of wave energy are 1.1×10^4 and 0.2×10^4 kWh/m, respectively. Zhou et al. [12] also calculated the total and exploitable storage of wave energy in the whole Beibu Gulf and showed that the highest total and exploitable storages are approximately 1.2×10^4 and 0.26×10^4 kWh/m which are nearly similar to the corresponding energy at station 5.

The second place with rich wave energy is station 4 with 0.88×10^4 and 0.13×10^4 kWh/m total and exploitable wave energies, respectively. The poorest storage of wave energy can be found at station 1 where the total and exploitable wave energies are only approximately 0.12×10^4 and 0.0005×10^4 kWh/m, respectively. Moreover, the total and exploitable wave energies at stations 2 and 3 are nearly similar (total: about 0.35×10^4 and 0.38×10^4 kWh/m, respectively and exploitable about 0.01×10^4 kWh/m).

These results indicate that the exploitable wave energy at station 5 is approximately 20 times greater than those of stations 2 and 3 and also is approximately 1.7 times greater than that of station 4. Therefore, station 5 which is located near Govatr port is suggested as the best location between the selected areas for wave energy extraction. The temporal-spatial distribution of the wave energy in northern coasts of Gulf of Oman indicates that the richest total and exploitable wave energy occurs at stations 4 and 5 located at the east of study area, during summer (June to August) with the dominant waves propagating from south to north.

Table 5. Total and exploitable storage of wave energy (*kWh/m*) per unit

Station no.	1	2	3	4	5
t_e	37.06	249.09	247.18	1266.69	1658.31
E_t	1217.39	3546.63	3768.51	8778.68	11170.04
E_e	5.15	100.85	106.34	1269.39	2114.54

4. Summary and Conclusions

In this study, wave energy obtained from the locally generated winds was assessed in the whole area and also five coastal stations in the northern Gulf of Oman, to locate the most appropriate locations for wave energy extraction. Wave data was obtained based on the numerical modeling using SWAN. Wind data used for wave modeling was ECMWF and measured wave data were used to calibrate and verify the numerical model. Regarding that the highest measured wave period was 8s in five weeks of measurement, swells were neglected and the model was calibrated and verified on order to simulate locally wind generated waves, accurately. Hence, the wave energy was estimated based only on the locally wind generated wave. After verifying the

SWAN model and running it for the period of 1992 to 2002, the wave power was calculated from the produced time series of wave characteristics. Spatial distribution of the wave power in the Gulf of Oman illustrates that the wave power increases from the Strait of Hormuz towards the Indian Ocean. Furthermore, the highest and lowest wave power values exist in summer and autumn, respectively.

Wave power potential was also assessed at five selected coastal stations located in northern areas of Gulf of Oman. Seasonal variations of the mean and maximum wave powers at the coastal stations show that the highest mean wave power occurs at the eastern station (station 5) in all seasons. In addition during autumn, winter and spring; the mean wave power increases gradually shifting from west to east while the increase of mean wave powers at stations 4 and 5 are considerable during summer, when the summer monsoon affects the east parts of the Gulf of Oman. Unlike the mean wave power, the maximum wave power is highest in winter at all stations. The results of monthly distribution of the wave power represent that the monthly mean wave power is highest during Jan to March at stations 1 to 3 and during June to August at stations 4 and 5, while the monthly maximum wave power is highest during February at all stations. There is an increase of maximum wave power in June at the western station (adjacent to the Persian Gulf) where the area is affected by Shamal winds.

Moreover, the highest and lowest monthly mean wave powers occur mostly at stations 5 and 1, respectively. The ratio of monthly maximum to mean wave power is the lowest during May to August. It varies slightly during these months, while the ratio increases during November and February at all stations, and also during April at stations 2 and 3 (middle stations). In addition, assessment of MVI shows that the highest value exists in the western part of the domain. The MVI firstly decreases and again increases moving from west to east, and station 3 has the lowest MVI.

Therefore, the most inappropriate place for wave energy extraction is suggested to be station 1 with the lowest wave energy and highest MVI. Furthermore, the dominant wave direction at most of the stations is S or SE in summer; mainly due to the waves coming from the Indian Ocean and it changes during the other seasons.

Analysis of inter-annual variation of the mean wave power represents that the annual variation of mean wave power is nearly similar to that of the spring, summer and autumn trends for these stations while the winter trend seems to be different from the other seasons. The results also indicate that the highest annual wave power occurs in station 5 in all years except for winter 1992, when the wave power is higher in station 2. The total and exploitable wave energy values were also estimated at different stations, and the results illustrate also that the richest wave energy can be found in the eastern part of the domain, where the total and exploitable storage of wave energy reaches 1.1×10^4 and 0.2×10^4 kWh/m, respectively.

Finally, it was shown that the richest area for wave energy extraction is station 5, located near Govatr port in the eastern part of the study area, and the highest energy exists during summer (when the energy demand is high) with the dominant waves propagating from the south. The second suitable station for wave energy extraction is station 4, which is located near Chabahar port and the poorest wave energy is located at station 1, at the west of the domain near the Strait of Hormuz, where the monthly variability index reaches the highest value.

Acknowledgement

The authors are thankful to SWAN groups at Delft University of Technology for making the model freely available.

References

[1] Leijon M, Bernhoff H, Berg M, Ågren O. Economical considerations of renewable electric energy production-especially development of wave energy. Renew Energy 2003;8:1201–9.

[2] Iglesias G, López M, Carballo R, , Castro A, Fraguela JA, Frigaard P. Wave energy potential in Galicia (NW Spain). Renew Energy 2009;34:2323-33.

[3] Gonçalves M, Martinho P, Guedes Soares C. Wave energy conditions in the western French coast. Renew Energy 2014;62:155–63.

[4] Sierra JP, González-Marco D, Sospedra J, Gironella X, Mösso C, Sánchez-Arcilla A. Wave energy resource assessment in Lanzarote (Spain). Renew Energy 2013;55:480-9.

[5] Iglesias G, Carballo R. Wave energy and nearshore hot spots: The case of the SE Bay of Biscay. Renew Energy 2010;35:2490-500.

[6] Pontes MT, Aguiar R, Pires HO. A nearshore wave energy atlas for Portugal. J Offshore Mech Arct 2005;127:249-55.

[7] Rusu E, Guedes Soares C. Numerical modelling to estimate the spatial distribution of the wave energy in the Portuguese nearshore. Renew Energy 2009;34:1501–16.

[8] Waters R, EngstrÖm J, Isberg J, Leijon M. Wave climate off the Swedish west coast. Renew Energy 2009;34:1600–6.

[9] Zodiatis G, Galanis G, Nikolaidis A, Kalogeri C, Hayes D, Georgiou GC, Chu PC, Kallos G. Wave energy potential in the Eastern Mediterranean Levantine Basin. An integrated 10-year study. Renew Energy 2014;69:311–23.

[10] Vicinanza D, Contestabile P, Ferrante V. Wave energy potential in the north-west of Sardinia (Italy). Renew Energy 2013;50:506-21.

[11] Mirzaei A, Tangang F, Juneng L Wave energy potential along the east coast of Peninsular Malaysia. Energy 2014;68:722-34.

[12] Zhou G, Huang J, Yue T, Luo Q, Zhang G. Temporal-Spatial distribution of wave energy: A case study of Beibu Gulf, China. Renew Energy 2015;74:344-56.

[13] Liang B, Fan F, Yin Z, Shi H, Lee D. Numerical modeling of the nearshore wave energy resources of Shandong peninsula, China. Renew Energy 2013;57:330-8.

[14] Sanil Kumar V, Anoop TR. wave energy resource assessment for the Indian shelf seas. Renew Energy 2015;76:212-9.

[15] Stopa JE, Cheung KF, Chen YL. Assessment of wave energy resources in Hawaii. Renew Energy 2011;36:554-67.

[16] Stopa JE, Filipot JF, Li N, Cheung KF, Chen YL, Vega L. Wave energy resources along the Hawaiian Island chain. Renew Energy 2013;55:305-21.
[17] Garcia-Medina G, Ozkan-Haller HT, Ruggiero P. Wave resource assessment in Oregon and southwest Washington, USA. Renew Energy 2014;64:203-14.
[18] Lenee-Bluhm P, Paasch R, Özkan-Haller HT. Characterizing the wave energy resource of the US Pacific Northwest. Renew Energy 2011;36:2106-19.
[19] Bernhoff H, Sjostedt E, Leijon M. Wave energy resources in sheltered sea areas: a case study of the Baltic Sea. Renew Energy 2006;31:2164-70.
[20] Kamranzad B, Etemad-Shahidi A, Chegini V. Wave energy assessment in the Caspian Sea. 18th congress of the IAHR-APD, Jeju, South Korea 2012;424-25.
[21] Haddadpour S, Etemad-Shahidi A, Kamranzad B. Wave energy forecasting using artificial neural networks in the Caspian Sea. Proc Ins Civil Eng-Mar En 2014;167:42–52.
[22] Hadadpour S, Etemad-Shahidi A, Jabbari E, Kamranzad B. Wave Energy and hot spots in Anzali port. Energy 2014;74:529–36.
[23] Rusu E, Onea F. Evaluation of the wind and wave energy along the Caspian Sea. Energy 2013;50:1-14.
[24] Etemad-Shahidi A, Kamranzad B, Chegini V. Wave energy estimation in the Persian Gulf. Proceedings of the International Conference on Environmental Pollution and Remediation, Canada 2011: no. 223.
[25] Kamranzad B, Etemad-Shahidi A, Chegini V. Assessment of wave energy variation in the Persian Gulf. Ocean Eng 2013;70:72-80.
[26] Saket A, Etemad-Shahidi A. Wave energy potential along the northern coasts of the Gulf of Oman. Renew Energy 2012;40:90-7.
[27] Booij N, Ris RC, Holthuijsen LH. A third-generation wave model for coastal regions. 1. Model Description and validation. J Geophys Res 1999;104:7649-66.
[28] Lin W, Sanford LP, Suttles SE. Wave measurement and modeling in Chesapeake Bay. Cont Shelf Res 2002;22:2673-86.
[29] Moeini MH, Etemad-Shahidi A, Chegini V. Wave modeling and extreme value analysis off the northern coast of the Persian Gulf. Appl Ocean Res 2010;32:209-18.
[30] Ris RC, Holthuijsen LH, Booij N. A third-generation wave model for coastal regions 2. Verification. J Geophys Res 1999;104:7667-81.

[31] Komen GJ, Hasselmann S, Hasselmann K. On the existence of a fully developed wind sea spectrum. J Phys Oceanogr 1984;14:1271-85.

[32] Abbaspour M, Rahimi R. Iran atlas of offshore renewable energies. Renew Energy 2011; 36:388-98.

[33] Moeini MH, Etemad-Shahidi A, Chegini V, Rahmani I. Wave data assimilation using a hybrid approach in the Persian Gulf. Ocean Dynam 2012;62:785-97.

[34] Moeini MH, Etemad-Shahidi A, Chegini V, Rahmani I, Moghaddam M. Error distribution and correction of the predicted wave characteristics over the Persian Gulf. Ocean Eng 2014;75:81-9.

[35] Rascle N, Ardhuin F. A global wave parameter database for geophysical applications. Part 2: Model validation with improved source term parameterization. Ocean Modelling 2013;70:174-88.

[36] Stopa JE, Cheung KF. Intercomparison of wind and wave data from the ECMWF Reanalysis Interim and the NCEP Climate Forecast System Reanalysis. Ocean Modelling 2014;75:65-83.

[37] Lv X, Yuan D, Ma X, Tao J. Wave characteristics analysis in Bohai Sea based on ECMWF wind field. Ocean Eng 2014; 91: 159-71.

[38] Henfridsson U, Neimane V, Strand K, Kapper R, Bernhoff H, Danielsson O, Leijon M, Sundberg J, Thorburn K, Ericsson E, Bergman K. Wave energy potential in the Baltic Sea and the Danish part of the North Sea, with reflections on the Skagerrak. Renew Energy 2007;32:2069-84.

[39] Hughes MG, Heap AD. National-scale wave energy resource assessment for Australia. Renew Energy 2010;35:1783-91.

[40] Thoppil PG, Hogan PJ. Persian Gulf response to a wintertime shamal wind event. J Deep-Sea Res I 2010;57:946-55.

[41] Cornett AM. A global wave energy resource assessment. International offshore and polar engineering conference, Vancouver, Canada 2008;318-26.

[42] Zheng CW, Pan J, Li JX. Assessing the China Sea wind energy and wave energy resources from 1988 to 2009. Ocean Eng 2013;65:39-48.

[43] Tsai CP, Hwang CH, Hwa C, Cheng HY. Study on the wave climate variation to the renewable wave energy assessment. Renew Energy 2012;38:50-61.

[44] Wen B, Xue YG, Zhang FR, Zhao CY. Numerical simulation of wave energy resources in the China Sea. Mar forecasts 2013;30:36-41.

Figures Caption

Black-and-white figures (for reproduction in print)

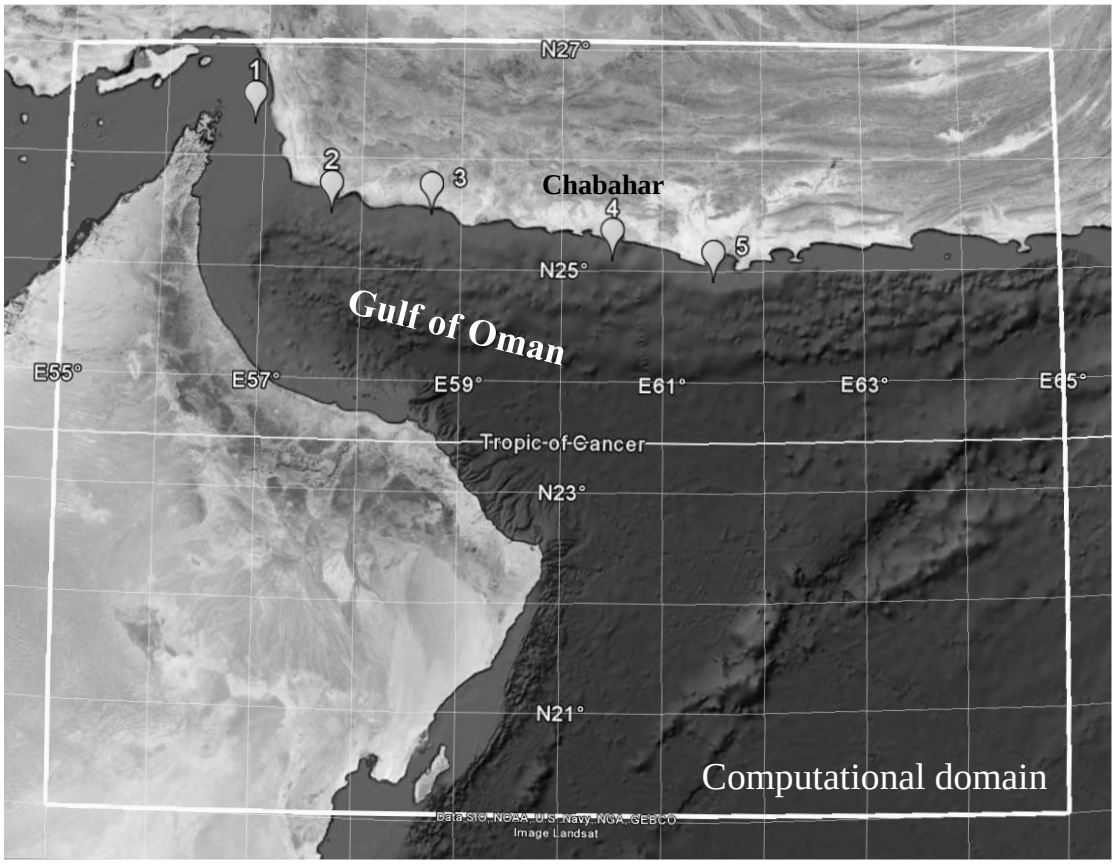

Fig. 1. Location of Gulf of Oman, computational grid and selected stations

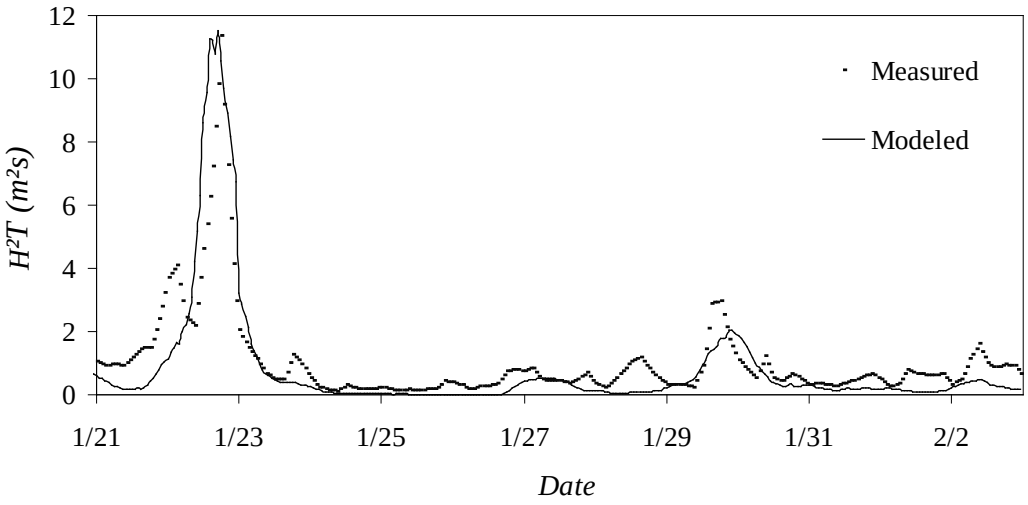

Fig. 2. Time series of modeled and measured H_s^2T, verification period

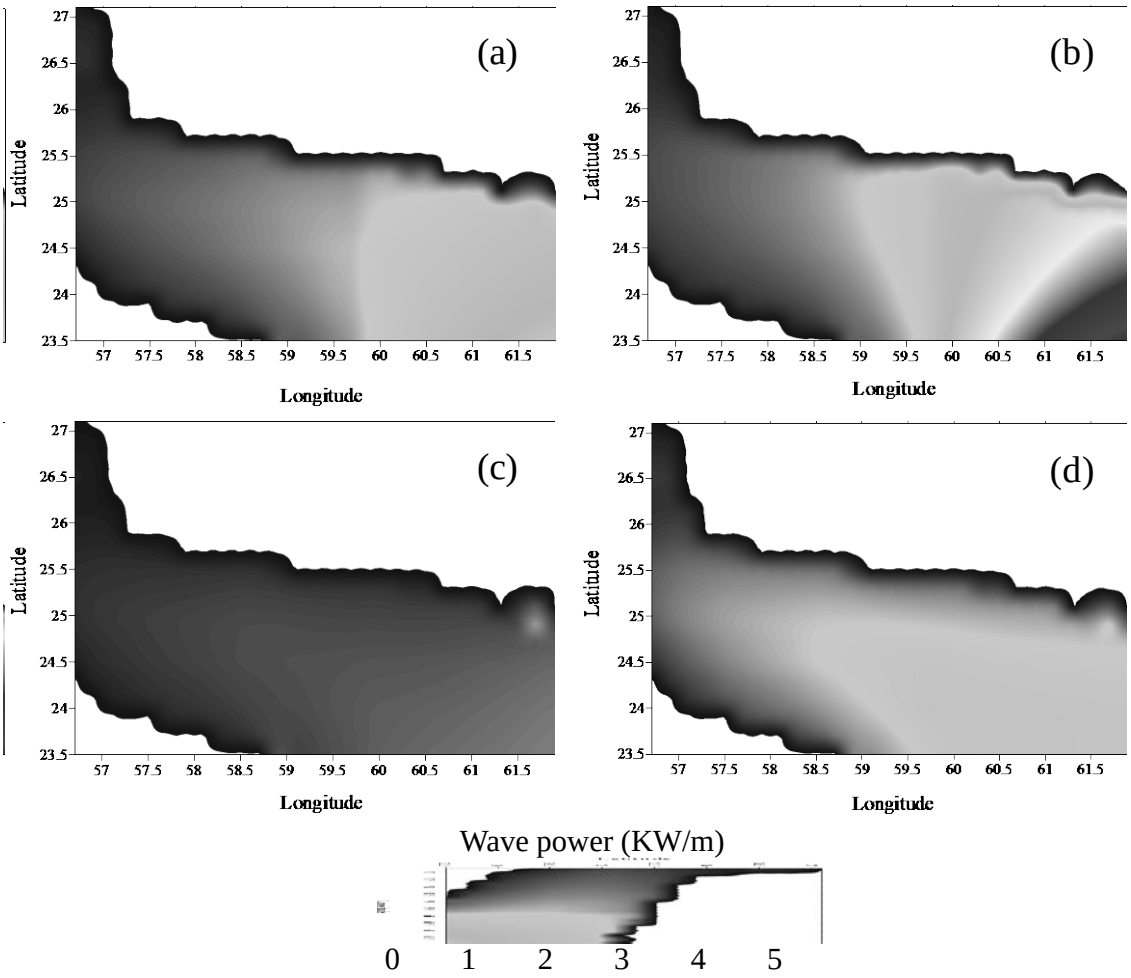

Fig. 3. Wave power (kW/m) distribution in Gulf of Oman in (a) Spring, (b) Summer, (c) Autumn and (d) Winter

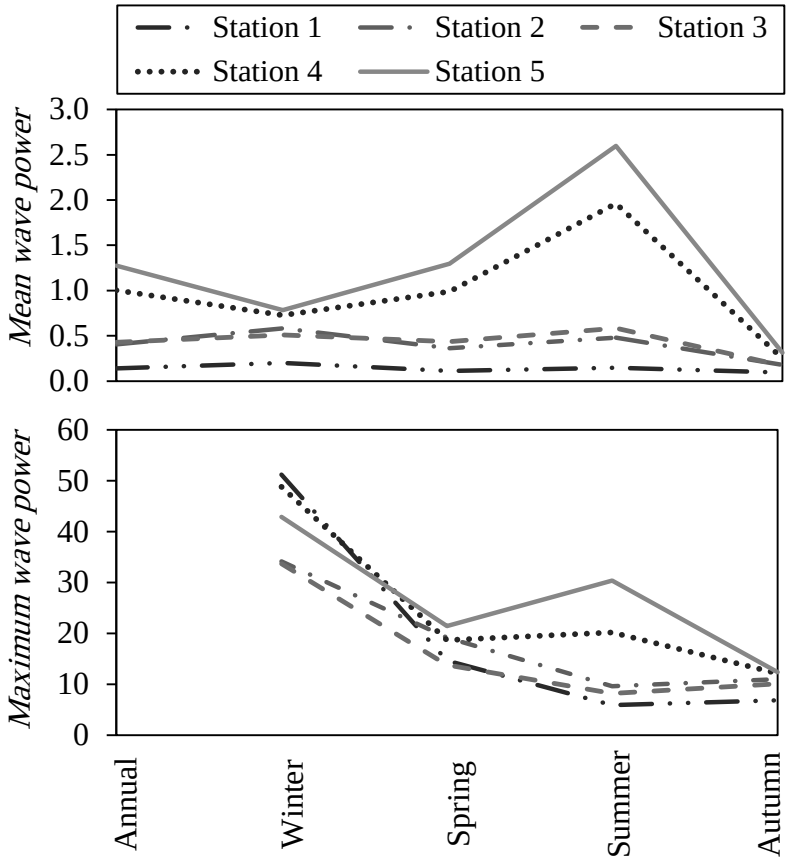

Fig. 4. Seasonal and annual distributions for (a) mean and (b) maximum wave power (kW/m)

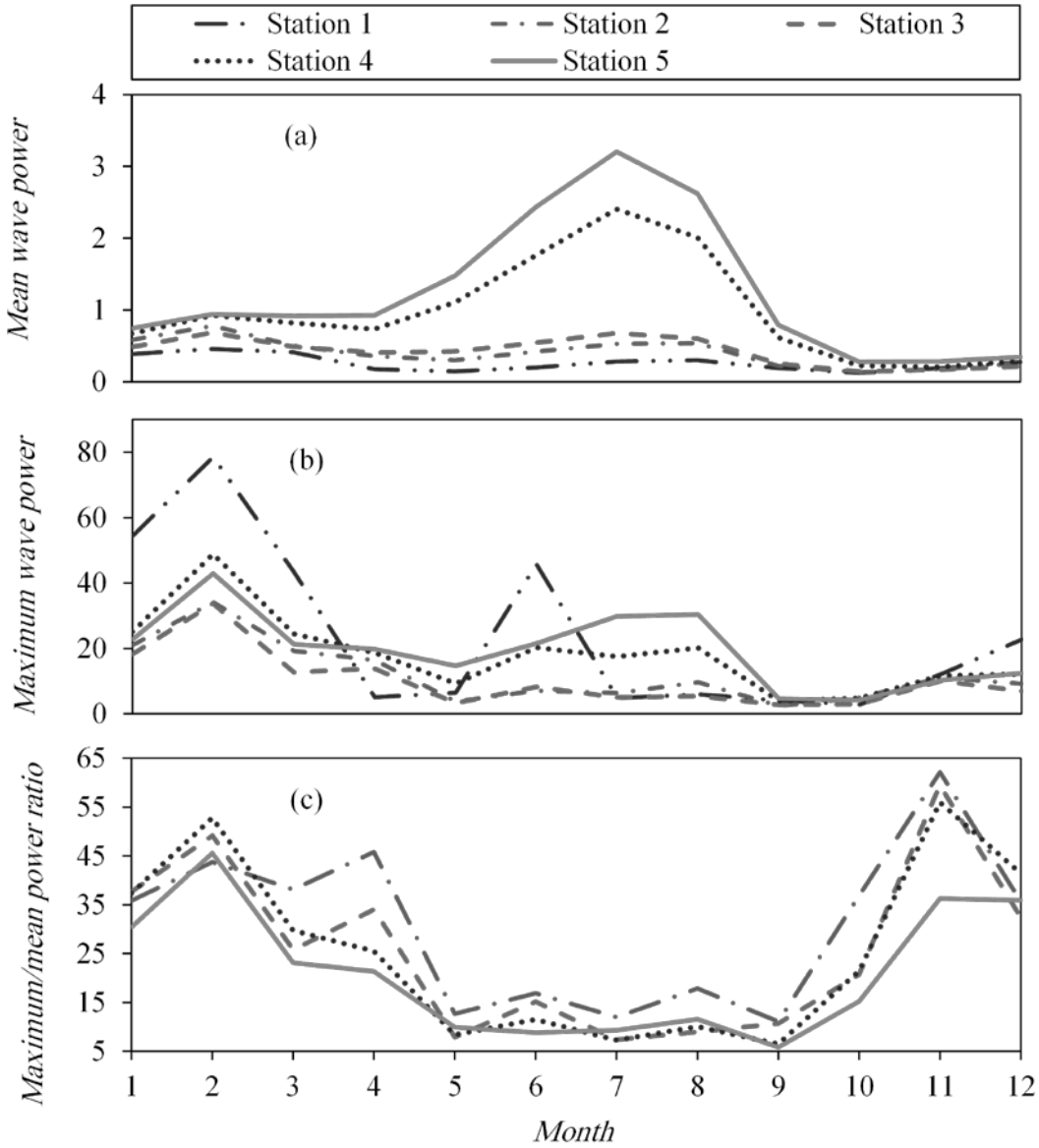

Fig. 5. Monthly distributions for (a) mean, (b) maximum and (c) ratio of Maximum/mean wave power (kW/m)

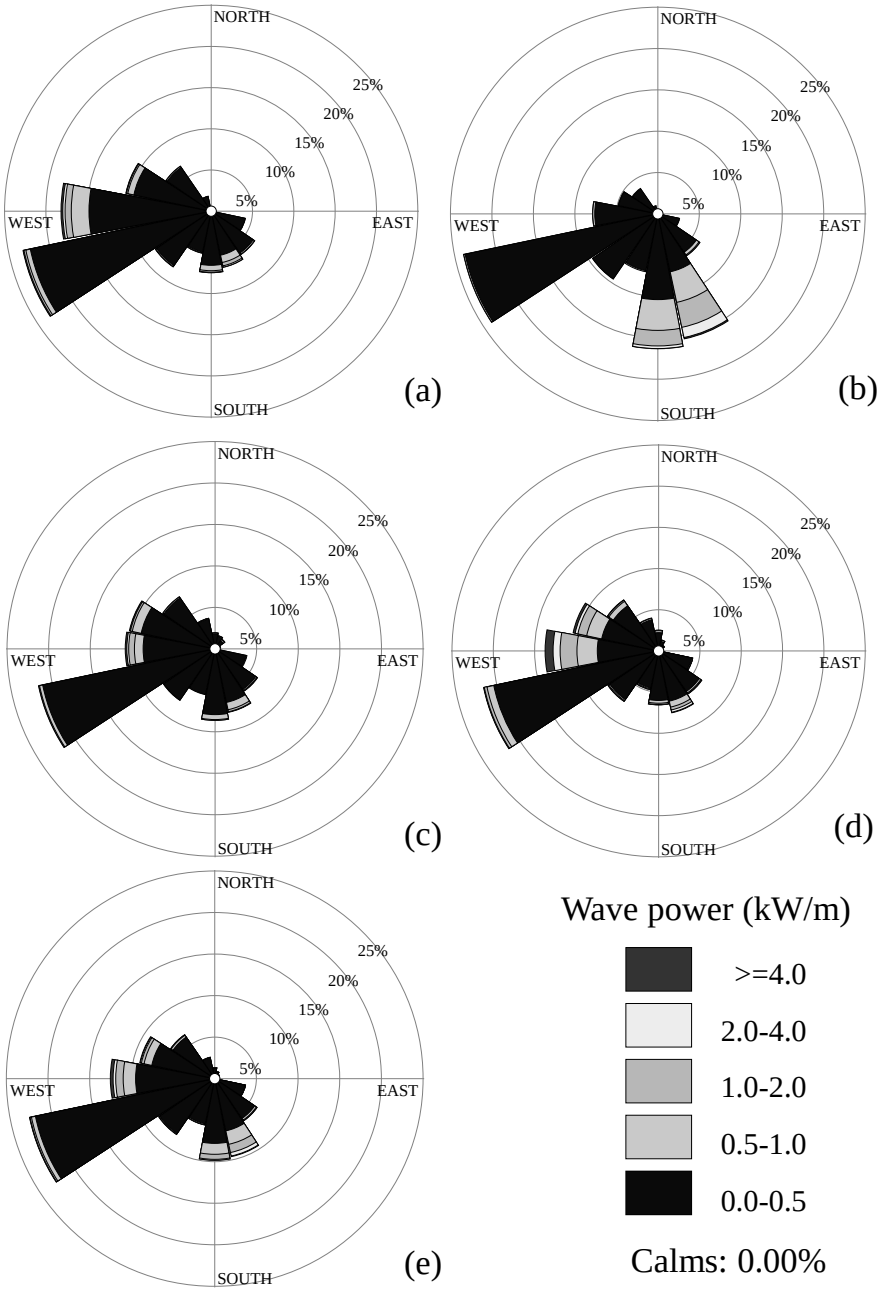

Fig. 6. Wave power roses, (a) spring, (b) summer, (c) autumn, (d) winter and (e) annual, in station 1

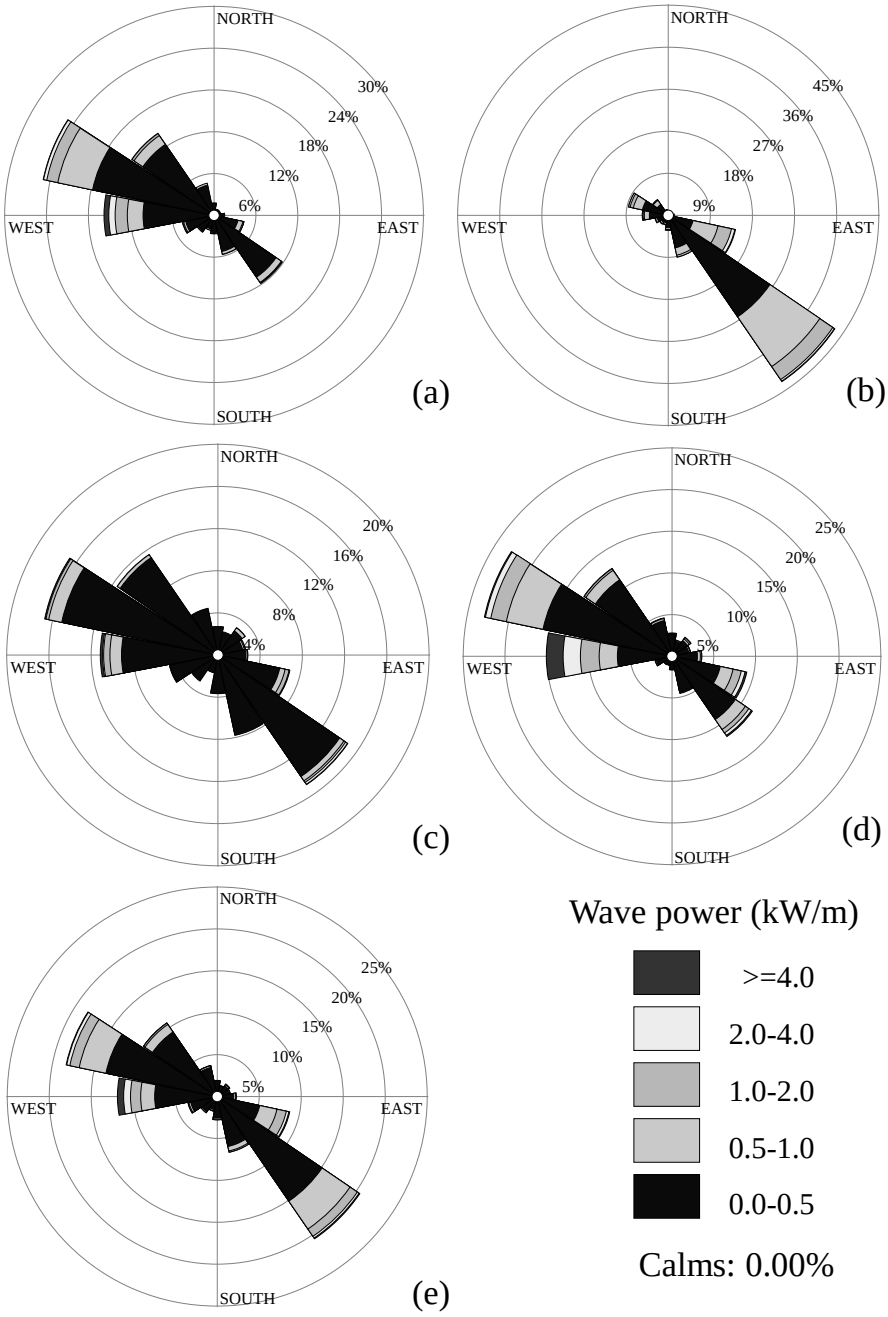

Fig. 7. Wave power roses, (a) spring, (b) summer, (c) autumn, (d) winter and (e) annual, in station 2

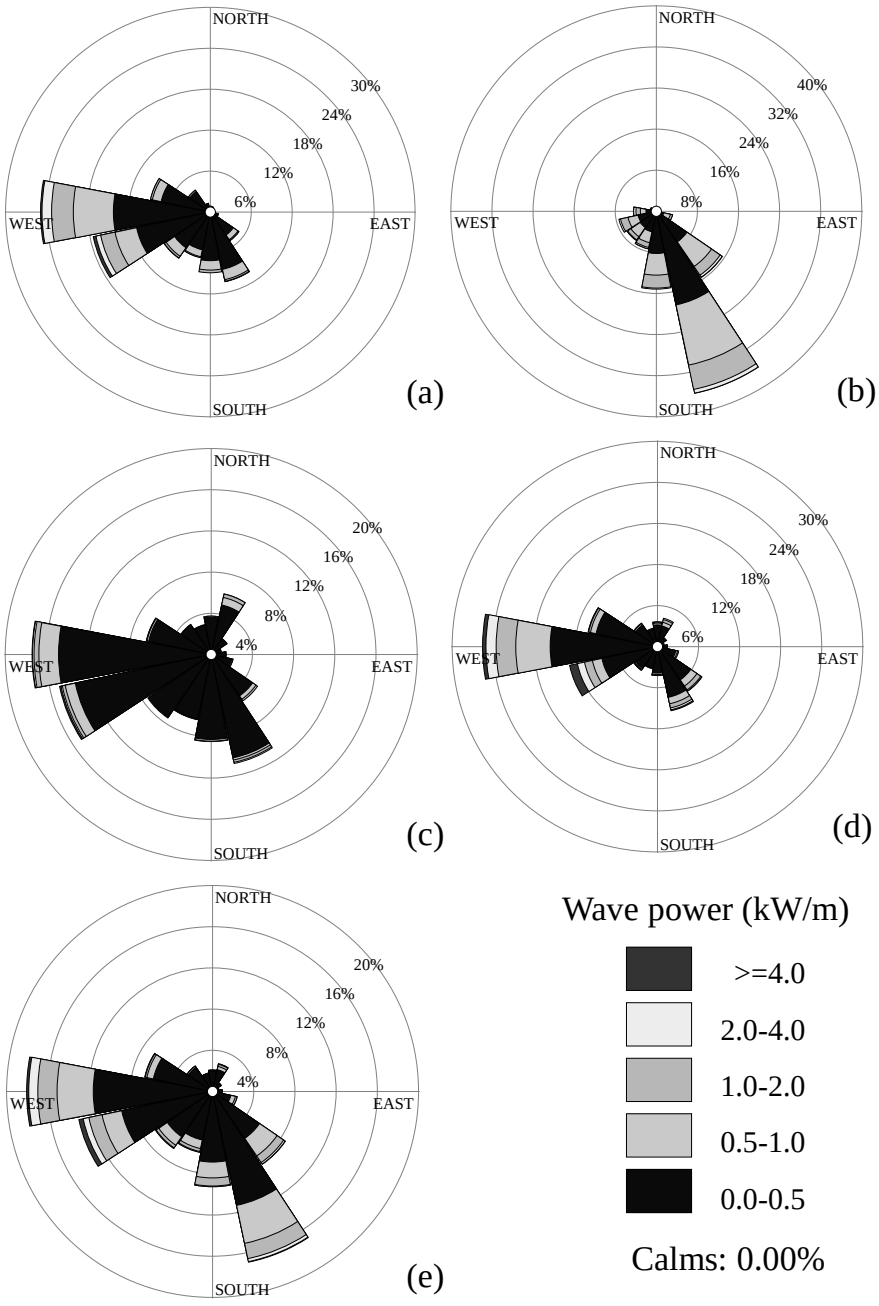

Fig. 8. Wave power roses, (a) spring, (b) summer, (c) autumn, (d) winter and (e) annual, in station 3

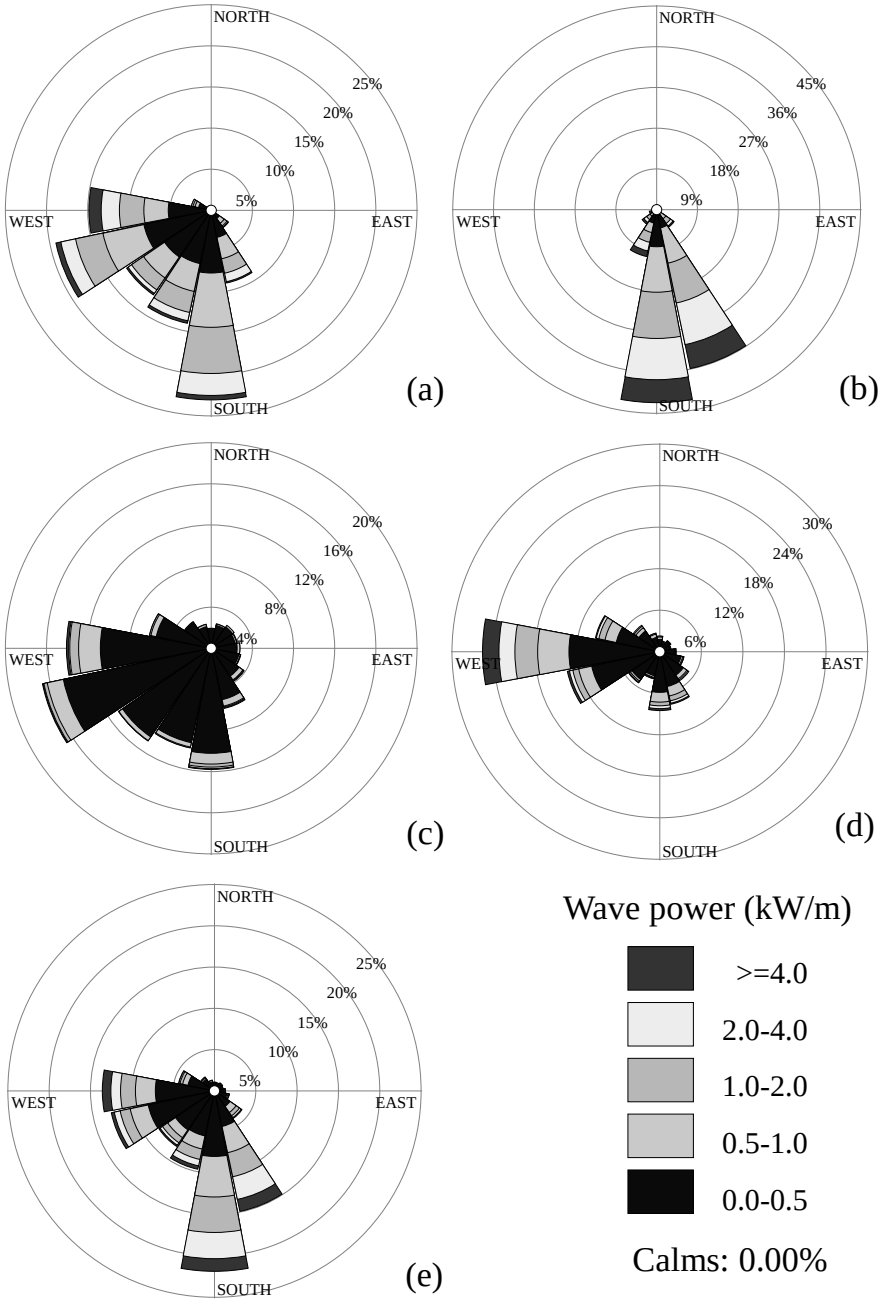

Fig. 9. Wave power roses, (a) spring, (b) summer, (c) autumn, (d) winter and (e) annual, in station 4

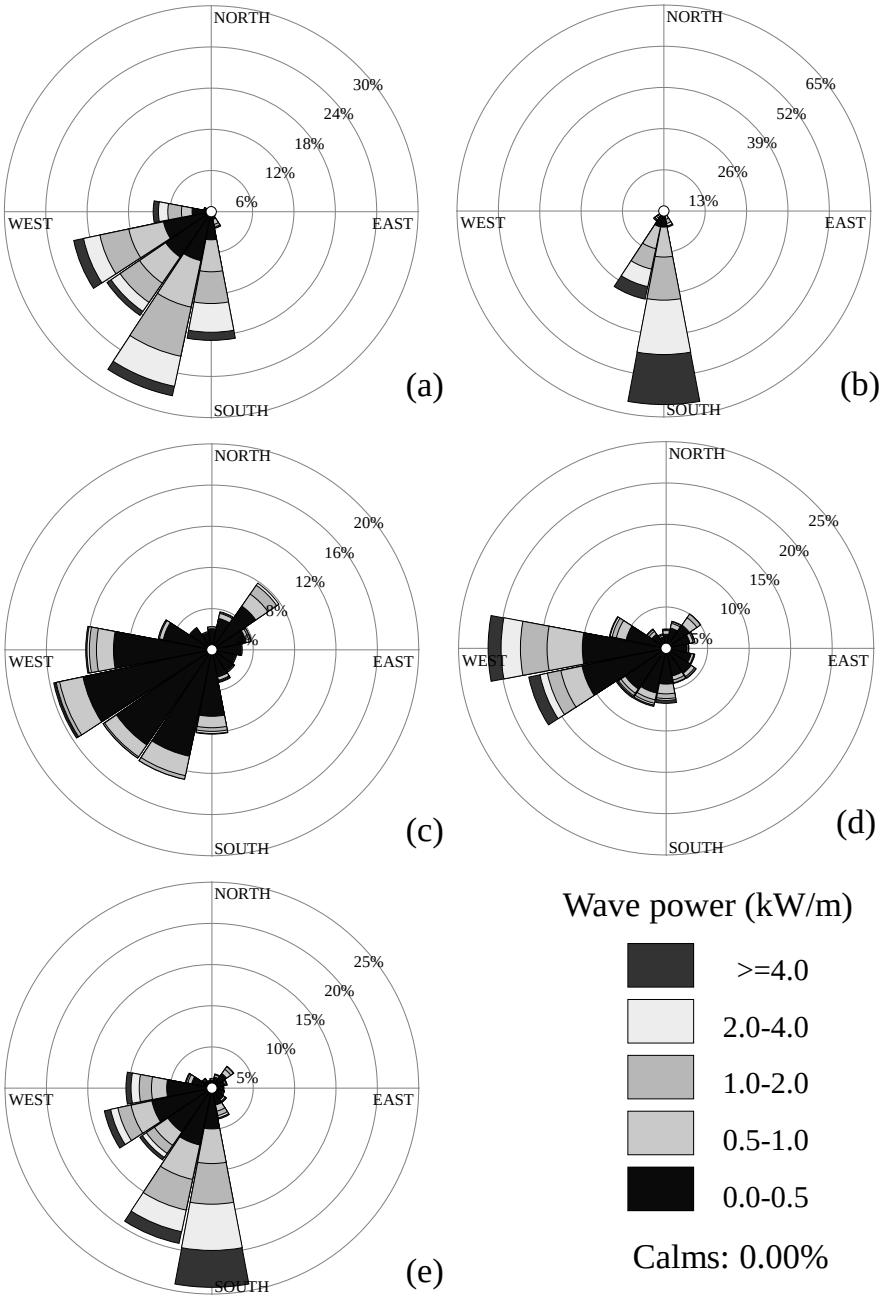

Fig. 10. Wave power roses, (a) spring, (b) summer, (c) autumn, (d) winter and (e) annual, in station 5

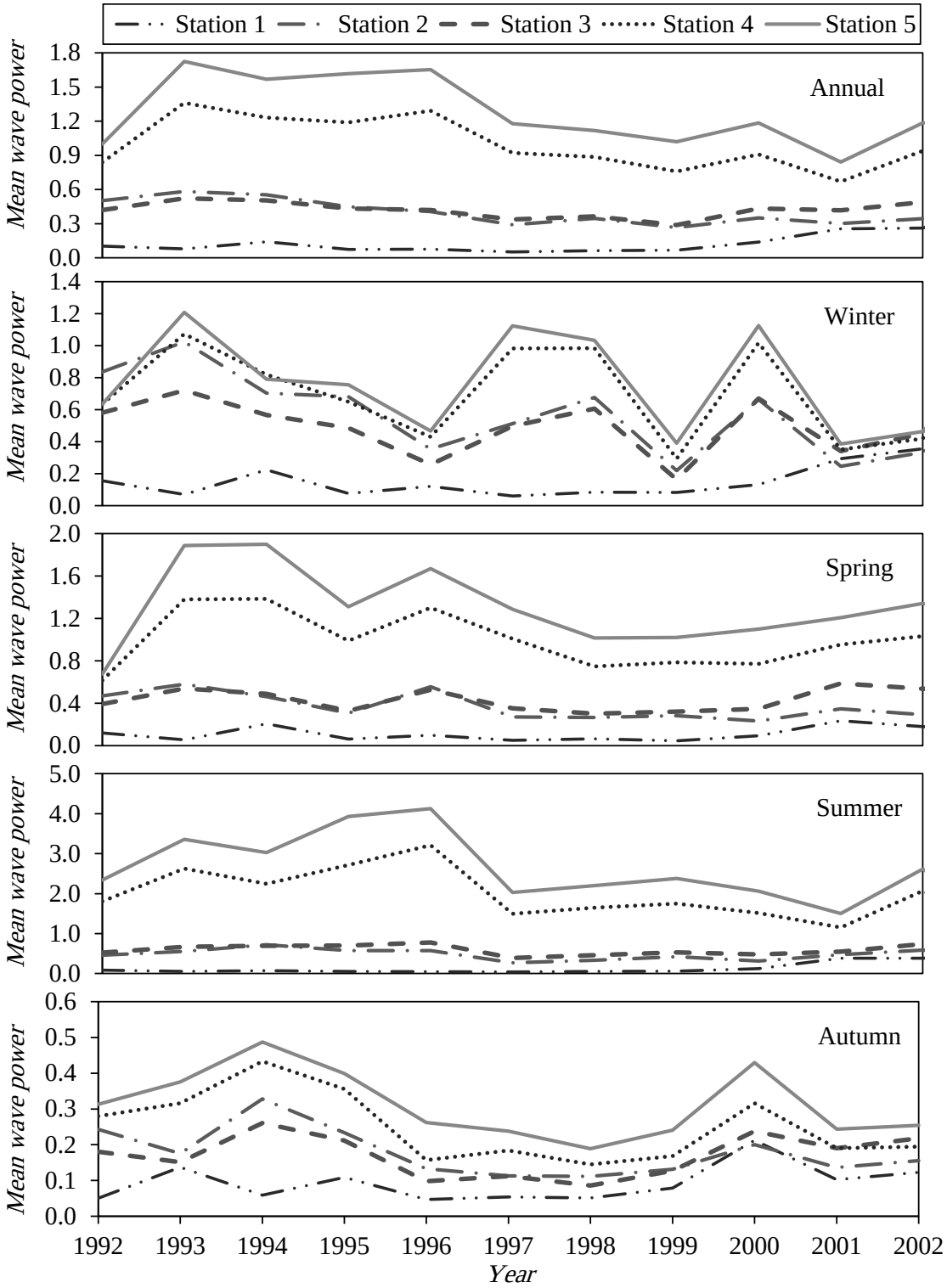

Fig. 11. Inter-annual distributions of seasonal mean wave power (kW/m)